Chapter 6

Enhanced Visible Light Photocatalytic Performance by Nanostructured Semiconductors with Glancing Angle Deposition Method

Shuang Shuang, Zheng Xie and Zhengjun Zhang

Additional information is available at the end of the chapter

http://dx.doi.org/10.5772/62890

Abstract

The glancing angle deposition (GLAD) method in physical vapor deposition is proved to be a versatile tool to fabricate nanostructured TiO_2 as the photocatalyst on specific substrates to form self-standing structures, which are much easier to be recycled. And novel designs of doping, decorating photocatalytic active substance, are brought in to make TiO_2 respond to visible light. In this chapter, we introduce our previous works such as TiO_2 nanorods with CdS quantum dots, noble metallic nanoparticles, coating TiO_2 via atomic layer deposition (ALD), and so on.

Keywords: Nanostructured, TiO_2, GLAD, visible light, degradation

1. Introduction

As we all know, population growth and rapid industrial development lead to global energy and environment crisis. However, sufficient utilization of solar energy could alleviate these issues, as the solar energy irradiating the surface of the Earth exceeds the current global human energy consumption by nearly four orders of magnitude. Thus, there has been keen interests in developing photocatalysts like semiconductors that can produce chemical energy from light. Semiconductor photocatalysis, which is regarded as a good candidate to convert renewable photon energy into chemical energy and decompose organic pollutants, has drawn much attention of researchers.

Since the first report of photocatalytic splitting over water taking use of TiO_2 photoanode by Fujisima and Honda in 1972 [1], TiO_2 has been widely studied and considered as one of the

superior candidates to settle the environmental concerns owing to its chemical inertness, low cost, photostability, nontoxicity and strong photocatalytic activity [2]. However, the industrial applications of it are also limited due to its large band gap (*ca*. 3.2 eV and 3.0 eV for anatase and rutile, respectively), which makes it to become active only under ultraviolet (UV) light (accounting for ~5% of the solar energy) [3]. And many efforts are made to enhance the photocatalytic performance of TiO_2 under visible lights range. So far, there are three main strategies to improve the photocatalytic efficiency and visible light utilization of TiO_2: (1) coupling with different semiconductors (e.g., TiO_2/Cu_2O [4] and TiO_2/WO_3 [5]), (2) combining with noble metals (e.g., Au/TiO_2 [6], Pt/TiO_2 [7] and Ag/TiO_2 [8, 9]), and (3) introducing dopants (e.g., oxygen defects [10], and sulfur [11], nitrogen [12]). Here, we will introduce these three methods in detail.

From previous studies, there are many methods to fabricate nanostructured materials. Among them, the glancing angle deposition (GLAD) technique is regarded as one simple but highly repeatable physical vapor deposition technology to prepare 1-dimensional and 2-dimensional nanomaterials, such as slanted posts, spirals, zigzag columns, nanopillars, etc. [13]. This method takes advantage of atomic shadowing and adatom diffusion to grow nanostructure materials. And these specific shaped nanostructures can be applied in many areas such as catalyst, optical element and magnetic storage media, etc. For instance, HfO_2 nanocolumn arrays can be applied as antireflection coating [14]. And altering GLAD fabrication conditions could also adjust relating the property parameter. Ag nanorod arrays (NRAs) could serve as surface-enhanced Raman scattering substrates. The limit Rhodamine 6G concentration of 10^{-14} mol/L can even be perceived using such kind of array structure. [15]

2. Doping

Traditional strategies in previous researches to broaden the solar spectral response of TiO_2 include surface sensitization by organic dyes and doping with transition metals. However, the commonly used dyes are in high price and the long-term stability of many dyes is also uncertain. Doping with transition metals makes the absorption shift to the visible region, even including all the solar spectra. While the metal ions could form recombination centers in the TiO_2 [16], which will reduce the efficiency of its photocatalytic activity.

Doping non-metal ion into TiO_2 may be a promising way to avoid the deterioration of the thermal stability of oxide lattice [17]. Many researchers reported doping experiments with various substances, such as nitrogen [18], sulfur [19] and fluoride [20] elements. Asahi et al. [21] reported that the band gap narrowed by N-doping, which improves the photocatalytic activity of TiO_2 under visible light irradiation. Since this work, such type of doping has been considered as one of the most effective approaches to shift the optical response of TiO_2 from the UV to the visible spectral range. There are mainly two major ways to prepare the N-doped TiO_2. One of them is using incorporation of N into TiO_2 lattice by ion-implantation technique, or other techniques, such as magnetron sputtering, hydrothermal method, etc. Another way, described in this work, relies upon the oxidation process of TiN_x, like powders and films prepared by these techniques.

http://dx.doi.org/10.5772/62890

2.1. Fabrication of N-doped TiO_2 NRAs

The TiN NRAs were deposited on F-doped SnO_2 (FTO) and quartz substrates through GLAD method. The substrate temperature was controlled at *ca*. −20°C by using liquid nitrogen to maintain the temperature. The N-doped TiO_2 NRAs were obtained by oxidizing the as-prepared TiN NRAs in a tube furnace under atmosphere at 330°C, and the N contents in TiO_2 NRAs were controlled by varying the annealing time (i.e., 5, 15, 30, 60 and 120 min). For the sake of convenience, one mark the TiN NRAs annealed for 5, 15, 30, 60 and 120 min as 5N-TiO_2, 15N-TiO_2, 30N-TiO_2, 60N-TiO_2 and 120N-TiO_2, respectively.

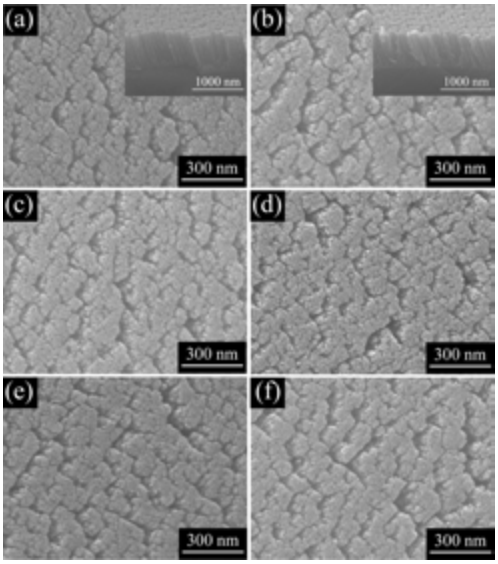

Figure 1. SEM images of the as-deposited TiN NRAs (a) 5N-TiO_2 NRAs (b), 15N-TiO_2 NRAs (c), 30N-TiO_2 NRAs (d), 60N-TiO_2 NRAs (e) and 120N-TiO_2 NRAs (f). The insets in (a) and (b) are the corresponding SEM images with a tilt angle of 45°.

Figure 1 is the scanning electron microscope (SEM) images of samples with various annealing time. Top-view image from **Figure 2(a)** shows that the as-prepared TiN NRAs exhibits porous structure. These nanorods (NRs) are found to be quite uniform with the length of ~600 nm, which are separated by voids as exhibited specially in the inset of **Figure 1(a)**. Moreover, it can be seen that the NRs are tilted with an angle of ~30° in the case of the substrate normal because of high angle of the incident adatom plume related to the substrate (α = 85°) [22]. The porous structure was also formed during the deposition process due to the self-shadowing effects and the limited mobility of the deposited atoms. The morphologies of the TiN NRAs annealed at 330°C for 5, 15, 30, 60 and 120 min do not change mainly and is corresponding with that of the as-deposited NRAs as exhibited in **Figures 1(b)–(f)**.

To study the microstructures of the as-prepared TiN NRAs and annealed samples furthermore, transmission electron microscope (TEM) is performed. **Figure 2(a)** shows the low-resolution TEM image of the TiN NRAs. It can be seen that the NR is of length ~600 nm and diameter of ~80 nm, which is in agreement with the SEM results. These pine needle structure NRs lead to an important enhancement in the total surface area, which is much higher than that of NRs with smooth surface. This microstructure can promote the performance of photoelectrochemistry because of the 1D structure with high specific surface area. **Figure 2(b)** exhibits the high-resolution TEM (HRTEM) image of the as-prepared TiN NRAs. The TiN crystalline grains can be observed clearly with interplanar lattice spacing of 0.212 nm, corresponding to (200) plane. TiN can be converted into TiO_2 by a complete oxidation at medium temperature in air condition. The oxidation occurs from the surface to the inner of NRs with diffusion of O_2. And the annealing time is also the critical parameter to decide the final oxidation degree. 15N-TiO_2 NRAs that annealed for 15 min at 330°C have huge amount of amorphous state, and only trace amount of TiO_2 crystalline grains with lattice spacing of 0.354 nm existed as shown in **Figure 2(c)**. Prolonging the annealing time to 120 min, huge amount of TiO_2 crystalline grains appeared and no TiN crystalline is found as shown in **Figure 2(d)**.

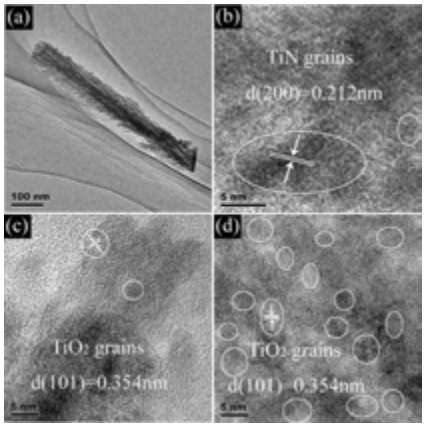

Figure 2. (a) Low-resolution cross-sectional TEM images of the as-prepared TiN NRAs; (b) HRTEM images of (a); (c) and (d) are the HR-TEM of the images of the 5N-TiO_2 NRAs and 120N-TiO_2, respectively.

Figure 3(a) exhibits the UV-visible light transmittance spectra of the TiN NRAs sample annealed during different time at 330°C. The as-prepared TiN films were assumed to be opaque with thickness of several tens of nanometers in previous report [23]; however, the transmittance of the as-prepared TiN NRAs actually in this study is ~25% under visible light test. With the increase in annealing time, the transmittance increases step by step at the wavelength of 300 to 600 nm, may due to the discrepancy in the degree of oxidation of the films from TiN to TiO_2. The spectra are studied by a high regularity of the interference fringes and a systematic increase in wavelength in which the film practically is no longer transparent in the visible range. This behavior has been previously found in TiO_2 doped with metals [24]. The optical

http://dx.doi.org/10.5772/62890

gap (E_g) of the semiconductor with large band gap can be calculated from the absorption coefficient α. The absorption coefficient can be expressed by, if scattering effect is neglected:

$$\left(\alpha E_g\right)^n = A\left(Eg - \hbar\upsilon\right), \tag{1}$$

where $n = 1/2$ is for an indirect transmission [25]. It could be assumed that the film contained both TiO_2 and TiN is the indirect semiconductor, similar with TiO_2. The Tauc plot of $(\alpha E)^{1/2}$ vs photon energy ($E = h\nu$) is shown in **Figure 3(b)**. Usually, the band gap can be gained by extrapolating the linear region to $(\alpha E)^{1/2}$=0. The band gap of the as-deposited TiN NRAs is *ca*. 1.49 eV. The band gap of the 120N-TiO_2 NRAs is 3.19 eV, which is very close to that of reported anatase TiO_2 (3.2 eV). It confirms that the TiN is turned to TiO_2 completely by annealing. The band gap varies from 1.49 to 3.19 eV with prolongation of annealing time. This result is pretty interesting from the photocatalysis viewpoint since it is possible to tune the onset of the absorption to the required visible wavelength range.

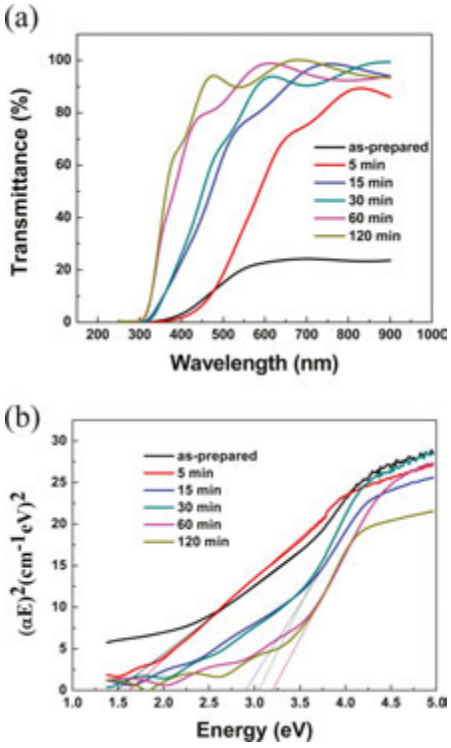

Figure 3. (a) Transmittance spectra of the doped samples annealed in different time; (b) Tauc plot of $(\alpha E)^{1/2}$ vs photon energy ($E = h\nu$) for the doped samples annealed for different time.

3. Coupling with other semiconductors

PbS [26], CdSe [27], ZnS [28] and CdS [29, 30] are semiconductors which own narrow band gap. They can be used as a sensitizer combined with TiO_2 to enhance the photocatalytic property. Especially, the band gap of CdS is about 2.4 eV which is of great advantage in photoelectrochemisty and photocatalysis [32]. Researchers have reported many works on growing CdS nanoparticles (NPs) on TiO_2 directly by chemical bath deposition (CBD) [34], electrodeposition [33] and successive ion layer adsorption and reaction (SILAR) [35, 36]. Improving electron-hole separation efficiency is beneficial for the photocatalytic performance [37]. Nano-sized TiO_2 is also good for reduction on recombining with photo-generated electrons [38]. What is more, nanostructured TiO_2 always shows various characteristics on property enhancement according to huge surface areas, high optical absorption degree and low reflectivity [39].

3.1. Decoration CdS NPs on TiO_2 NRAs

3.1.1. Fabrication of TiO_2 NRAs

Choosing FTO and Si as substrates to deposit Ti NRAs using GLAD technique, in which the morphology of nanostructure was investigated by SEM. Firstly, clean the substrates sequentially in acetone, alcohol and deionized water by ultrasonic, respectively, and each for 5 min. Then, the as-prepared samples were oxidized from Ti NRAs to TiO_2 NRAs using tube furnace of 450°C for 2 hrs with a rate of 5°C min^{-1} in air.

3.1.2. CdS NPs deposition on TiO_2 substrates

CdS NPs deposited TiO_2 NRAs by SILAR method have been reported previously [30, 46]. TiO_2 NRAs substrates were alternatively dipped in $Cd(Ac)_2$ and Na_2S solutions each for 30 s to react with CdS nanostructure for each time. They were also rinsed in deionized water between every solutions for 30 s. The SILAR process was repeated until it reached the satisfied cycle numbers.

Top-view SEM image of Ti NRAs is showed in **Figure 4(a)** and the insert picture exhibits tilted angle-view SEM image of the samples. And the Ti NRs are uniformed with ~70 nm in diameter, ~220 nm in length. The top-view SEM image of oxide sample was exhibited in **Figure 4(b)** which kept the similar dimensions and sample compared to Ti NRAs. **Figure 4(c–f)** are the top-view SEM images of CdS deposition samples with 5, 10, 15 and 20 SILAR cycles. SILAR method has been used in previous research and it is thought as an effective way to synthesis of CdS [47]. Large CdS particles were formed after 15 cycles, and after 20 cycles CdS particles even aggregated with each other.

http://dx.doi.org/10.5772/62890

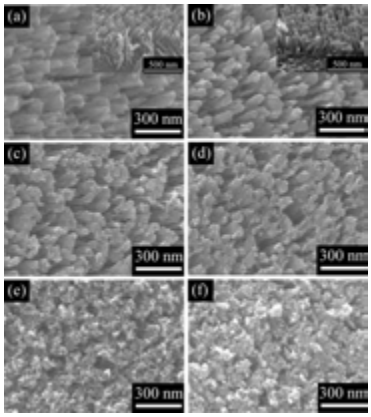

Figure 4. SEM images of the as-prepared samples: (a) Ti NRAs; (b) TiO_2 NRAs sample, the insets in (a) and (b) are the images recorded at a tilt angle of 45°; CdS deposition with cycle number of (c) 5, (d) 10, (e) 15, and (f) 20 SILAR.

Different cycle numbers of CdS SILAR coating on TiO_2 NRs were observed by HRTEM technology. The morphology of TiO_2 NRs are exhibited in **Figure 5(a–b)**. It can be seen that TiO_2 NRs are polycrystalline which contain two phases (anatase and the rutile). And the heterojunction of these two phases could block recombination of electrons and holes [48]. HRTEM images of 15 cycles CdS NPs decoration are shown in **Figure 5(c–d)**. And we can see that the average diameter of CdS NPs is ~5 nm, which attach to TiO_2 NRs forming heterojunctions of TiO_2 and CdS. And large amount of CdS wraps up TiO_2 NRs when cycle number reaches to 25.

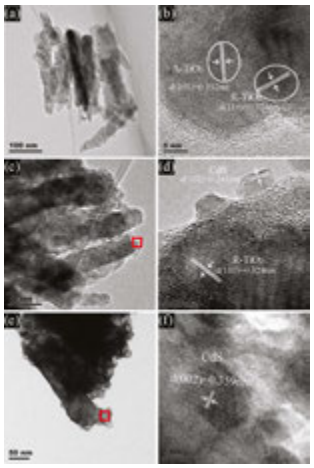

Figure 5. TEM images and HRTEM images: (a, b) TiO_2 NRAs; (c, d) 15 SILAR cycles TiO_2 NRAs/ CdS NPs; (e, f) 25 SILAR cycles TiO_2 NRAs/CdS NPs.

Discoloration of methyl orange (MO) under visible light of different SILAR cycle numbers is measured to test its photocatalytic performance. As we all know, the absorbance peak intensity of the λ = 462 nm is proportional to the concentration of MO solution [49]. And the reaction rate η can be computed by

$$\eta = 1 - \frac{A(t)}{A_0}, \tag{2}$$

where A_o and $A(t)$ are absorbance intensity values at the 0 and t reaction time, respectively.

Discoloration rate of prepared samples with the irradiation time is exhibited in **Figure 6**. It can be seen that discoloration rate of pure TiO_2 NRAs was only 3.2% just due to photobleaching process [50]. Then with the increase in SILAR cycle number, the discoloration rate improved first and then reduced. Specially, when cycle number is 20, it showed the best photocatalytic performance which reached to 42.0% after 150 min irradiation.

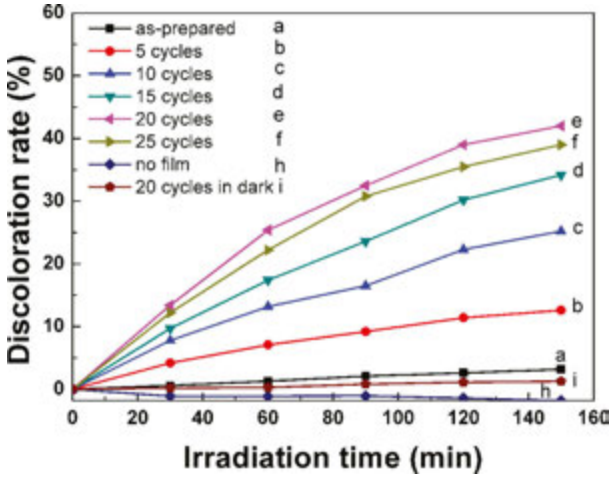

Figure 6. Visible light ($\lambda \geq 420$ nm) discoloration of MO of samples.

When visible light irradiate on materials, the CdS reacted due to the narrow band gap and produce electrons and holes. What is more, CdS decorated with TiO_2 NRAs also reduced the happening of recombination because of band gap matching, thus improving the photocatalytic performance. The electrons accumulated at the conduction band (CB) of semiconductors change to active oxygen species (*e.g.*, $\cdot O_2^-$) with oxygen, which could also participate in discoloration [51]. Meantime, the formed hydroxyl radicals ($\cdot$OH) could also help break down organic molecule. Holes produced in the valence band of CdS often take part in decomposition to let the dye turn to intermediates or mineralized products [52]. Thus, the addition of CdS is

http://dx.doi.org/10.5772/62890

beneficial to the enhancement of MO discoloration in a degree. The whole reaction process is shown in **Figure 7**.

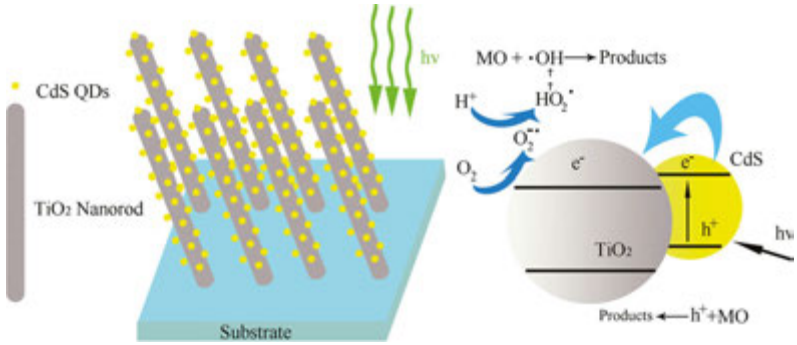

Figure 7. Schematic of degradation process of MO process for TiO_2 NRAs/CdS NPs.

3.2. TiO_2 NRAs/CdS quantum dots by coating TiO_2 *via* atomic layer deposition (ALD)

One big disadvantage of CdS QDs is that the excited electrons and holes of CdS QDs will be trapped by the surface states in ambient conditions. This problem causes the degradation of photostability and photocatalytic efficiency. Hence, it is crucial to reduce the recombination of electrons and holes, in order to improve the photostability of CdS and enhance the photocatalytic efficiency [53]. One effective way to decrease the surface recombination velocity is to fabricate a surface coating on CdS QDs. ALD is a kind of coating technique to deposit a very thin film that could passivate the surface states and then reduce the surface recombination velocity. The layer-by-layer deposition allows highly conformal coating even on the dense and rough surface of certain nanostructures. In previous study, ALD technique has had success in preventing anodic corrosion on other nanostructured materials [54].

Here, a TiO_2 NRAs/CdS QDs/ALD-TiO_2 composite material is investigated. The TiO_2 NRAs were also made by GLAD method, while the CdS QDs and the ultra-thin TiO_2 film were coated alternatively by SILAR and ALD technique, respectively. Outstanding photocatalytic property and stability were achieved in this kind of structure, which predicts huge potency on solar energy conversion.

3.2.1. Fabrication ALD on TiO_2 NRAs

The substrate temperature of ALD was controlled at 150°C during the coating process. Four dimethylamino titanium, the precursor, was maintained at 110°C and water at 40°C. N_2 was assumed as purge and carrier gas. To guarantee enough penetration of the precursors into the whole NRs, a soak step was taken, which is very similar to that adopted in previous study [55, 56]. First, four dimethylamino titanium was pulsed for 250 ms and kept for additional 5 s, and then the chamber was evacuated. After that H_2O was pulsed in for 5 ms and allowed to soak

for another 3 s, followed by a 20 s purge step. This process was repeated until the demanded deposition of TiO_2 was complicated.

The typical top-view SEM image of 5 SILAR cycles CdS QDs decoration was showed in **Figure 8(a)**, and the inset image of the NRs with a tilt angle of 45°. The uniform NRAs are about ~70 nm in diameter, and ~220 nm in length, while the CdS QDs deposited on TiO_2 NRAs are rather small with size below 20 nm. **Figure 8(b–f)** show the top-view SEM images of the TiO_2 NRAs/CdS QDs coated with TiO_2 layers by 20, 40, 60, 80 and 160 ALD cycles, respectively. Specially, there is no obvious change in morphology when the ALD cycles are less than 80.

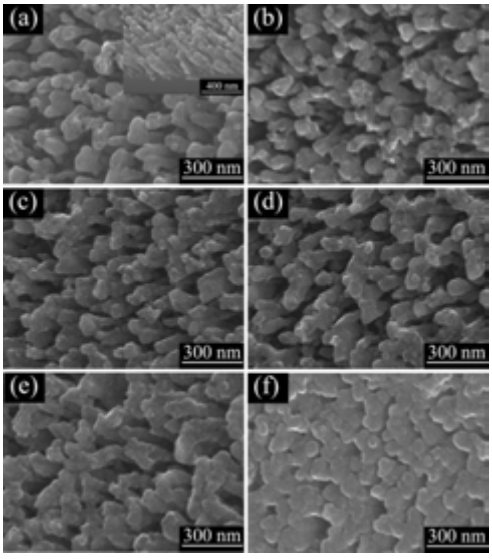

Figure 8. SEM images of the samples: (a) TiO_2 NRAs/CdS QDs, inset is the image with a tilt angle of 45°; TiO_2 NRAs/CdS QDs coated with ALD TiO_2 with different cycles: (b) 20 cycles; (c) 40 cycles; (d) 60 cycles; (e) 80 cycles; (f) 160 cycles.

The TiO_2 layers deposited on TiO_2 NRAs/CdS QDs by ALD were studied in detail by HRTEM technique. **Figure 9(a–b)** are the images of TiO_2 NRAs/CdS QDs before coating with TiO_2 layer. The TiO_2 NRs are in polycrystalline state with the length of ~220 nm and diameter of ~50 nm, which is corresponding with SEM results. Ultrafine CdS QDs with diameter of ~3 nm are coated on TiO_2 NRs, making up the CdS/TiO_2 heterojunction. **Figure 9(c–d)** are the HRTEM images of TiO_2 NRAs/CdS QDs decorated with 60 ALD cycles TiO_2 layer (i.e., TiO_2 NRAs/CdS QDs/60c-ALD-TiO_2). It is obvious that an ultrathin amorphous TiO_2 layer (~2 nm thick) was deposited completely and uniformly on the TiO_2 NRAs/CdS QDs, forming another CdS/TiO_2 heterojunction. Furthermore, **Figure 9(e–f)** exhibit the TEM images of TiO_2 NRAs/CdS QDs/80c-ALD-TiO_2, and the thickness of the amorphous TiO_2 layer is ~2.8 nm which can be seen clearly in the HRTEM image corresponding to **Figure 9(f)**.

http://dx.doi.org/10.5772/62890

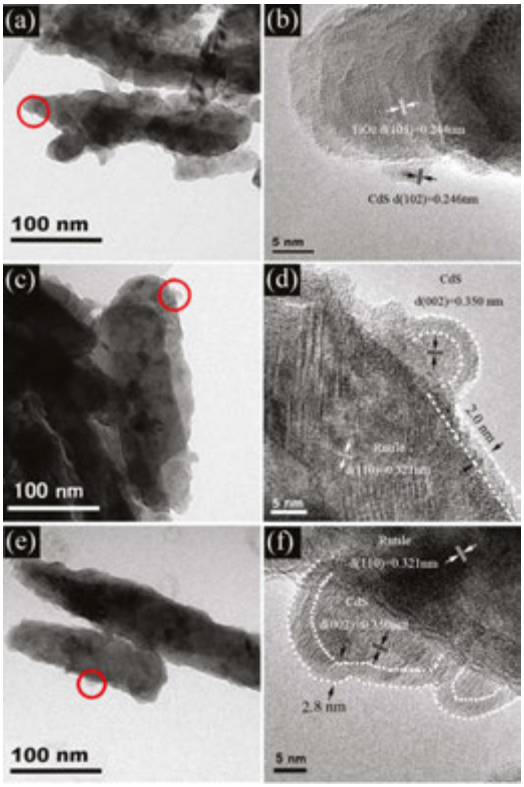

Figure 9. TEM images and HRTEM images: (a, b) TiO_2 NRAs/CdS QDs; TiO_2 NRAs/CdS QDs coated with ALD TiO_2 with various cycles: (c, d) for 60 and (e, f) for 80 cycles.

We also test the photocatalytic performance of composite materials by the photodegradation experiments of MO under visible light irradiation. It is also following the Beer's law as introduced previously [49]. **Figure 10** shows the degradation rate of MO after 1 h irradiation under visible light range, choosing TiO_2 NRAs/CdS QDs/ALD-TiO_2 as the photocatalyst. The degradation rate is only 2.92% when choosing TiO_2 NRAs/CdS QDs without coating ALD TiO_2. And enhancement of degradation rate occurred when taking TiO_2 NRAs/CdS QDs/ALD-TiO_2 as the photocatalyst.

For instance, the degradation rate was 4.16% for TiO_2 NRAs/CdS QDs/20c-ALD-TiO_2, and it promoted 7.47% for TiO_2 NRAs/CdS QDs/60c-ALD-TiO_2, in which the rate improved 156% compared to that of TiO_2 NRAs/CdS QDs in the absence of coating. However, it is also obvious that when taking the TiO_2 NRAs/CdS QDs/80c-ALD-TiO_2 and TiO_2 NRAs/CdS QDs/160c-ALD-TiO_2 as photocatalysts, the degradation rate of both decreases greatly. The annealed samples exhibit similar catalytic performance without obvious variation of degradation between the annealed and the original samples.

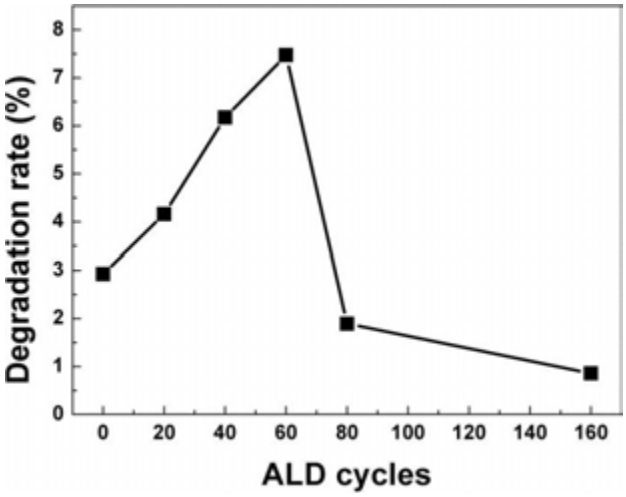

Figure 10. Visible light ($\lambda \geq 420$ nm) degradation behavior of MO using TiO_2 NRAs/CdS QDs/ALD-TiO_2 as catalyst.

4. Coupling with noble metal

Combining with metal is a promising method to develop highly efficient visible light photocatalyst. On one hand, the deposition of the metal on TiO_2 can greatly improve its photoefficiency through the Schottky barrier CB electron trapping and consequent longer electron-hole pair lifetime [57]. Hu et al. [58] reported a highly efficient Pt-doped TiO_2 which have enhanced photocatalytic activity for NO_x oxidation both under UV and visible light irradiation. Ingram et al. managed to reduce the high rate of charge-carrier recombination by combining a semiconductor photocatalyst with tailored plasmonic-metal nanostructures [59]. The presence of Pt deposited on TiO_2 is believed to retard the rapid charge-pair recombination by serving as an electron sink and facilitating interfacial electron transfer to dioxygen or other electron acceptors. Pt can also trap electrons on the CB, which are subsequently transferred to electron acceptors [60]. On the other hand, some noble metal NPs, such as Ag and Au, exhibit strong UV-vis absorption due to their plasmon resonance, produced by the collective oscillations of surface electrons. Pu et al. demonstrated those Au NPs, Au NRs and a mixture of Au NPs and NRs on the surface of TiO_2 nanowire arrays could be prepared for effective photocatalysis and the activities were enhanced in both the UV and the visible regions [61].

Despite these promising studies, combining the plasmonic effect of Au and electron sink effect of Pt has not been reported so far to our knowledge. Furthermore, photocatalysts in previous reports were usually in the form of powders and in an amorphous state, which was hard to handle and restricted its practical applications. In the present work, we designed a plasmonic photocatalyst consisting of bimetallic Au-Pt/TiO_2 supported on specific SiO_2 substrates. Firstly, the vertically aligned TiO_2 NRAs were fixed on specific SiO_2 substrates by GLAD technique.

http://dx.doi.org/10.5772/62890

Then, the Au and Pt NPs were deposited on TiO_2 by using SILAR method. Excellent photocatalytic property and stability were achieved and the fabrication of TiO_2 self-standing structures, which will be easier for recycling and thus facilitating their potential applications in solar energy-driven photocatalysis.

4.1. Metallic NPs deposition on TiO_2 NRAs

Au/Pt NPs were deposited on TiO_2 NRs through SILAR method with slight modification as previously reported [30]. Briefly, the TiO_2 NRAs substrates were successively exposed to $HAuCl_4$ (or HPt_2Cl_6) and $NaBH_4$ solutions to deposit nanocrystallites. The TiO_2 NRAs were immersed in 0.1 mg/mL $HAuCl_4$ (or 0.1 mg/mL HPt_2Cl_6) solution for 60 s, followed by rinsing with DI water and then immersed in $NaBH_4$ solution (1 mg/mL) for another 60 s, after which the resultant was rinsed with DI water for several times. This SILAR process was repeated for several cycles until the desired quantity of metallic nanocrystallites was achieved. Here, Au/Pt-TiO_2 sample was alternately coated with Au and Pt NPs, respectively, for 5 times.

Figure 11 presents the X-ray diffraction (XRD) patterns of different samples. All samples exhibited diffraction peaks at 25.2° and 27.3° corresponding to the (101) crystal planes of the anatase phase (JCPDS No. 21–1272) and (110) crystal planes of the rutile phase (JPCDS No. 21–1276). Besides this, the diffraction peaks (38.2°, 41.4°) assigned to Au (JCPDS No. 04–0784) and the peak at 39.7° assigned to Pt (JCPDS No. 04–0802) were displayed in Au-TiO_2 and Pt-TiO_2, respectively. These three peaks were also observed in Au/Pt-TiO_2 sample.

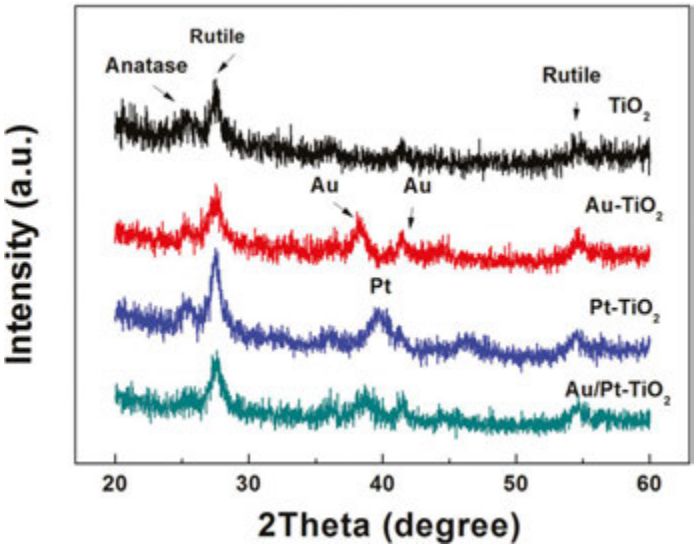

Figure 11. XRD patterns of the Au/TiO_2 NRAs coated with 10 cycles, Pt/TiO_2 NRAs coated with 10 cycles and Au/Pt/TiO_2 NRAs.

Figure 12 shows the SEM images of the pure TiO_2 film and those coated with Au, Pt and Au/Pt NPs with 10 cycles, respectively. As-annealed film consists of vertically aligned TiO_2 NRs with a diameter of ~50 nm and a length of ~200 nm (**Figure 12(a)**). Au and Pt NPs distribute uniformly on the TiO_2 NRAs surface (**Figure 12(d) and 12(c)**).

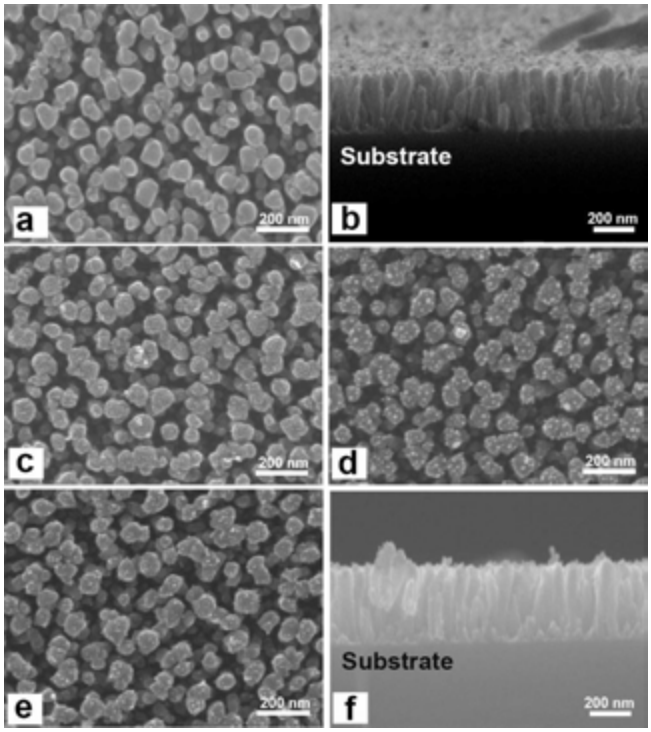

Figure 12. SEM images of the different samples: (a) TiO_2 NRAs; (b) cross-section of TiO_2 NRAs; (c) Pt-TiO_2 NRAs coated with 10 cycles; (d) Au-TiO_2 NRAs coated with 10 cycles; (e) Au/Pt-TiO_2 NRAs; (f) cross-section of sample Au/Pt-TiO_2 NRAs.

Furthermore, TEM images in **Figure 13** show that Au and Pt were uniformly dispersed on the surface of TiO_2. Their average sizes were about ~4 nm, and in a regular cubic shape. According to the measurement of lattice fringes, d = 0.23, 0.24, 0.34 and 0.32 nm match very well with the crystallographic planes of Pt (111), Au (111), anatase (101) and rutile (110), respectively. This result indicated that Au, Pt and TiO_2 were effectively interfaced. The formation of metal-semiconductor nanojunctions, including Au-TiO_2 and Pt-TiO_2, could be favorable for interfacial charge transfer among the three components, enhancing photocatalytic activities of the composites. In addition, the existence of anatase-rutile heterojunction in the NRs may help the rutile particles to efficiently collect photon-induced electrons from the anatase particles to reduce the carrier recombination [48].

http://dx.doi.org/10.5772/62890

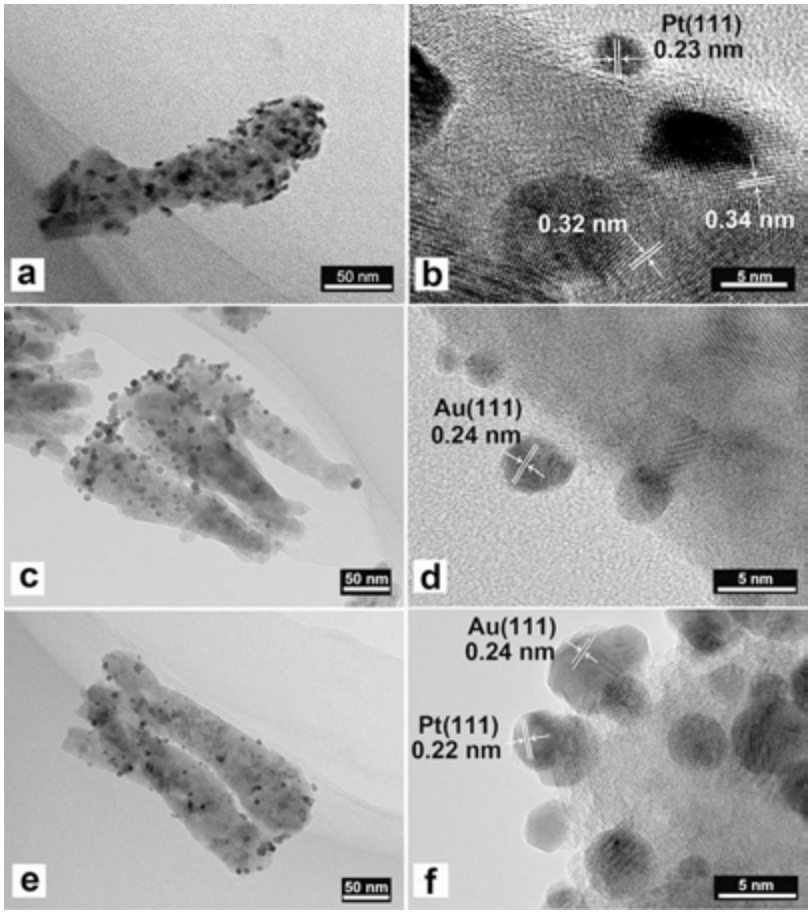

Figure 13. TEM images and HRTEM images of (a–b) Pt/TiO_2 NRAs coated with 10 cycles; (c–d) Au/TiO_2 NRAs coated with 10 cycles; (e–f) $Au/Pt/TiO_2$ NRAs.

To evaluate the effect of bimetal Au-Pt on the photocatalytic activity of TiO_2, the photodegradation of MO was carried out under visible irradiation. As a comparison, MO degradation were also performed in Pt/TiO_2, Au/TiO_2 and TiO_2. As shown in **Figure 14**, neither TiO_2 nor $Pt\text{-}TiO_2$ showed any activity for the MO degradation, while 20% MO was degraded by $Au\text{-}TiO_2$ after 120 illumination under otherwise condition. In the range of wavelength $\lambda > 420$ nm, only Au NPs have light absorption, and the degradation of MO in $Au\text{-}TiO_2$ is from the plasmon-induced Au NPs. Moreover, the rate of MO photodegradation on $Au/Pt\text{-}TiO_2$ was 1.36 times faster than that on $Au\text{-}TiO_2$. Therefore, Pt NPs also played an important role in the enhanced activity of $Au\text{-}Pt/TiO_2$. Compared with the photocurrent of $Au\text{-}TiO_2$, which of $Au\text{-}Pt/TiO_2$ was remarkably enhanced, indicating that the latter sample exhibited higher charge separation efficiency.

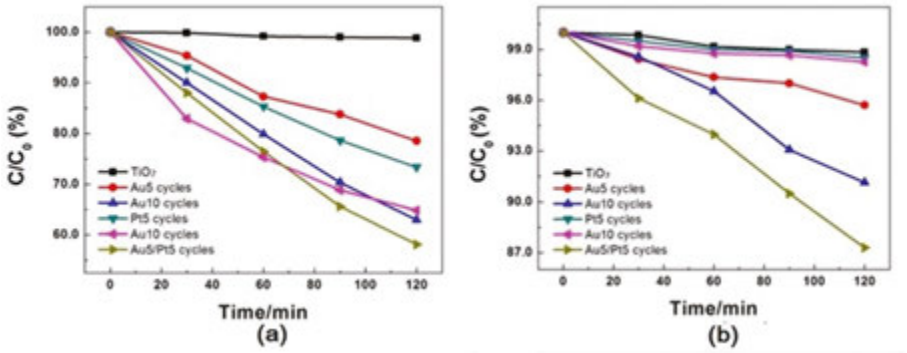

Figure 14. UV-vis light discoloration of (a) MO and (b) current versus time measurements; visible light (λ ⊚ 420 nm) discoloration of (c) MO and (d) current versus time measurements.

Surface plasmon resonance (SPR) peak wavelength of Au NPs in visible light region is ~520 nm. And the incident photons are absorbed by Au NPs through SPR excitation [62]. Soon afterwards, hot electrons move from the plasmon-excited Au to the CB of TiO_2 [63]. And then electrons transfer from CB to Pt due to the work function of Pt larger than Au. Here, Pt NPs take part in the process as cocatalyst at which electrons could react with electron acceptors (O_2 absorbed on the surface of Ti^{3+} or dissolved in water) to create superoxide radicals ($O_2^{\bullet-}$). At the meantime, the resultant electron-deficient Au particles can oxidize the organic molecule or react with OH^- to form hydroxyl radicals, OH•, which are highly oxidizing species. The process is shown in **Figure 15**. And co-decoration of Au/Pt not only improves the efficiency of charge separation, improving its photocatalytic efficiency, but also expands the active range of TiO_2 to visible light region. What is more, it was also verified that active radicals produced from UV-photoexcited TiO_2 create electron-hole pairs reacting with adsorbed oxygen/H_2O [65]. As a result, the highly efficient degradation of dyes came from both photoexcited TiO_2 and plasmon-excited Au NPs under UV irradiation.

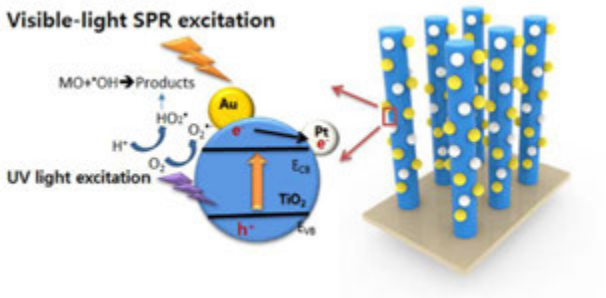

Figure 15. The photocatalytic process for Au/Pt/TiO_2 NRAs under UV-vis lights.

http://dx.doi.org/10.5772/62890

5. Summary

In this chapter is introduced three main methods of coupling with different semiconductors, combining with noble metals and introducing dopants to make TiO_2 be active in visible light region. Our studies demonstrate that through rational design of composite nanostructures, one can achieve on utilizing a high-energy photon under sunlight. And combining different materials together, which matches their bands with each other and with various nanostructures, could both eventually realize higher efficiency of solar spectrum.

Author details

Shuang Shuang[1], Zheng Xie[1,3] and Zhengjun Zhang[2*]

*Address all correspondence to: zjzhang@tsinghua.edu.cn

1 State Key Laboratory of New Ceramics and Fine Processing, School of Materials Science and Engineering, Tsinghua University, Beijing, China

2 Key Laboratory of Advanced Materials (MOE), School of Materials Science and Engineering, Tsinghua University, Beijing, China

3 High-Tech Institute of Xi'an, Xi'an, China

References

[1] Fujishima A, Honda K. Electrochemical photolysis of water at a semiconductor electrode. Nature. 1972;238(5358):37–38. DOI: 10.1038/238037a0

[2] Yuan RS, Chen T, Fei EH, Lin JL, Ding ZX, Long JL, et al. Surface chlorination of TiO2-based photocatalysts: a way to remarkably improve photocatalytic activity in both UV and visible region. Acs Catal. 2011;1(3):200–206. DOI: 10.1021/cs100122v

[3] Barborini E, Conti AM, Kholmanov I, Piseri P, Podesta A, Milani P, et al. Nanostructured TiO2 films with 2 eV optical gapsDOI. Adv Mater. 2005;17(15):1842–1846. DOI: 10.1002/adma.200401169

[4] Zhang JY, Zhu HL, Zheng SK, Pan F, Wang TM. TiO2 Film/Cu2O microgrid heterojunction with photocatalytic activity under solar light irradiation. Acs Appl Mater Inter. 2009;1(10):4207–4209 . DOI: 10.1063/1.1426256

[5] Higashimoto S, Sakiyama M, Azuma M. Photoelectrochemical properties of hybrid WO3/TiO2 electrode. Effect of structures of WO3 on charge separation behavior. Thin Solid Films. 2006;503(1–2):201–206. DOI: 10.1016/j.tsf.2005.11.110

[6] Tian Y, Tatsuma T. Mechanisms and applications of plasmon-induced charge separation at TiO2 films loaded with gold nanoparticles. J Am Chem Soc. 2005;127(20):7632–7633. DOI: 10.1021/ja042192u

[7] Low CTJ, de Leon CP, Walsh FC. The reduction of hydrogen peroxide at an Au-coated nanotubular TiO2 array. J Appl Electrochem. 2014;44(1):169–177. DOI: 10.1007/s10800-013-0623-5

[8] Hirakawa T, Kamat PV. Photoinduced electron storage and surface plasmon modulation in Ag@TiO2 clusters. Langmuir. 2004;20(14):5645–5647. DOI: 10.1021/la048874c

[9] Akhavan O. Lasting antibacterial activities of Ag-TiO2/Ag/a-TiO2 nanocomposite thin film photocatalysts under solar light irradiation. J Colloid Interf Sci. 2009;336(1):117–124. DOI: 10.1016/j.jcis.2009.03.018

[10] Ihara T, Miyoshi M, Ando M, Sugihara S, Iriyama Y. Preparation of a visible-light-active TiO2 photocatalyst by RF plasma treatment. J Mater Sci. 2001;36(17):4201–4207. DOI: 10.1023/A:1017929207882

[11] Umebayashi T, Yamaki T, Itoh H, Asai K. Band gap narrowing of titanium dioxide by sulfur doping. Appl Phys Lett. 2002;81(3):454–456. DOI: 10.1063/1.1493647

[12] Miyauchi M, Ikezawa A, Tobimatsu H, Irie H, Hashimoto K. Zeta potential and photocatalytic activity of nitrogen doped TiO2 thin films. Phys Chem Chem Phys. 2004;6(4):865–870. DOI: 10.1039/b314692h

[13] Qin Z, Zhengcao L, Jie N, Zhengjun Z. A simple model to describe the rule of glancing angle deposition. Mater Transac 2011;52(3):469–473. DOI: 10.2320/matertrans.M2010342

[14] Jie N, Yu Z, Qin Z, Zhengjun Z. Morphology in-design deposition of HfO2 thin films. 2008;91:3458–3460. DOI: 10.1111/j.1551-2916.2008.02654.x

[15] Chaney SB, Shanmukh S, Dluhy RA, Zhao YP. Aligned silver nanorod arrays produce high sensitivity surface-enhanced Raman spectroscopy substrates. 2005;87(3): DOI: 10.1063/1.1988980

[16] Herrmann JM, Disdier J, Pichat P. Effect of chromium doping on the electrical and catalytic properties of powder titania under UV and visible illumination. Chem Phys Lett. 1984;108(6):618–622. DOI: 10.1016/0009-2614(84)85067-8

[17] Yin S, Aita Y, Komatsu M, Sato T. Visible-light-induced photocatalytic activity of TiO2-xNy prepared by solvothermal process in urea-alcohol system. J Eur Ceram Soc. 2006;26(13):2735–2742. DOI: 10.1016/j.jeurceramsoc.2005.05.012

[18] Shieh DL, Lin YS, Yeh JH, Chen SC, Lin BC, Lin JL. N-doped, porous TiO2 with rutile phase and visible light sensitive photocatalytic activity. Chem Commun. 2012;48(19):2528–2530. DOI: 10.1039/c2cc16960f

[19] Ohno T, Akiyoshi M, Umebayashi T, Asai K, Mitsui T. Preparation of S-doped TiO2 photocatalysts and their photocatalytic activities under visible light. Appl Catal a-Gen. 2004;265(1):115–121. DOI: 10.1016/j.apcata.2004.01.007

[20] Ho W, Yu JC, Lee S. Synthesis of hierarchical nanoporous F-doped TiO2 spheres with visible light photocatalytic activity. Chem Commun. 2006;10:1115–1117. DOI: 10.1039/b515513d

[21] Asahi R, Morikawa T, Ohwaki T, Aoki K, Taga Y. Visible-light photocatalysis in nitrogen-doped titanium oxides. Science. 2001;293(5528):269–271. DOI: 10.1126/science.1061051

[22] Wolcott A, Smith WA, Kuykendall TR, Zhao YP, Zhang JZ. Photoelectrochemical water splitting using dense and aligned TiO2 nanorod arrays. Small. 2009;5(1):104–111. DOI: 10.1002/smll.200800902

[23] Van Bui H, Groenland AW, Aarnink AAI, Wolters RAM, Schmitz J, Kovalgin AY. Growth kinetics and oxidation mechanism of ALD TiN thin films monitored by in situ spectroscopic ellipsometry. J Electrochem Soc. 2011;158(3):H214–H220. DOI: 10.1149/1.3530090

[24] Pereira ALJ, Gracia L, Beltran A, Lisboa PN, da Silva JHD, Andres J. Structural and electronic effects of incorporating Mn in TiO2 films grown by sputtering: anatase versus rutile. J Phys Chem C. 2012;116(15):8753–8762. DOI: 10.1021/jp210682d

[25] Miyata N, Akiyoshi S. Preparation and electrochromic properties of Rf-sputtered molybdenum oxide-films. J Appl Phys. 1985;58(4):1651–1655. DOI: 10.1063/1.336307

[26] Lee H, Leventis HC, Moon SJ, Chen P, Ito S, Haque SA, et al. PbS and CdS quantum dot-sensitized solid-state solar cells: old concepts, new results. Adv Func Mater. 2009;19(17):2735–2742. DOI: 10.1021/la900247r

[27] Lee HJ, Bang J, Park J, Kim S, Park S-M. Multilayered semiconductor (CdS/CdSe/ZnS)-sensitized TiO2 mesoporous solar cells: all prepared by successive ionic layer adsorption and reaction processes. Chem Mater. 2010;22(19):5636–5643. DOI: 10.1021/cm102024s

[28] Guijarro N, Campiña JM, Shen Q, Toyoda T, Lana-Villarreal T, Gómez R. Uncovering the role of the ZnS treatment in the performance of quantum dot sensitized solar cells. Phys Chem Chem Phys. 2011;13(25):12024–12032. DOI: 10.1039/c1cp20290a

[29] Li G-S, Zhang D-Q, Yu JC. A new visible-light photocatalyst: CdS quantum dots embedded mesoporous TiO2. Environ Sci Technol. 2004;43(18):7079–7085. DOI: 10.1039/c3nr34253k

[30] Baker DR, Kamat PV. Photosensitization of TiO2 nanostructures with CdS quantum dots: particulate versus tubular support architectures. Adv Func Mater. 2009;19(5):805–811. DOI: 10.1002/adfm.200801173

[31] Das K, De S. Optical properties of the type-II core-shell TiO2@ CdS nanorods for photovoltaic applications. J Phys Chem C. 113(9):3494–501. DOI: 10.1039/c4ra01769b

[32] Liu Y, Zhou H, Zhou B, Li J, Chen H, Wang J, et al. Highly stable CdS-modified short TiO_2 nanotube array electrode for efficient visible-light hydrogen generation. Int J Hydrogen Energy. 2011;36(1):167–174. DOI: 10.1016/j.ijhydene.2010.09.089

[33] Wang C, Sun L, Yun H, Li J, Lai Y, Lin C. Sonoelectrochemical synthesis of highly photoelectrochemically active TiO2 nanotubes by incorporating CdS nanoparticles. Nanotechnology. 2009;20(29):295601. DOI: 10.1088/0957-4484/20/29/295601

[34] Lin S-C, Lee Y-L, Chang C-H, Shen Y-J, Yang Y-M. Quantum-dot-sensitized solar cells: assembly of CdS-quantum-dots coupling techniques of self-assembled monolayer and chemical bath deposition. Appl Phys Lett. 2007;90(14):143517–143530. DOI: 10.1063/1.2721373

[35] Luo J, Ma L, He T, Ng CF, Wang S, Sun H, et al. TiO2/(CdS, CdSe, CdSeS) nanorod heterostructures and photoelectrochemical properties. J Phys Chem C. 2012;116(22): 11956–11963. DOI: 10.1021/jp3031754

[36] Cheng S, Fu W, Yang H, Zhang L, Ma J, Zhao H, et al. Photoelectrochemical performance of multiple semiconductors (CdS/CdSe/ZnS) cosensitized TiO2 photoelectrodes. J Phys Chem C. 2012;116(3):2615–2621. DOI: 10.1021/jp209258r

[37] Shaislamov U, Yang BL. CdS-sensitized single-crystalline TiO2 nanorods and polycrystalline nanotubes for solar hydrogen generation. J Mater Res. 2013;1(1):1–6. DOI: 10.1557/jmr.2012.373

[38] Salvador P. Hole diffusion length in n-TiO 2 single crystals and sintered electrodes: photoelectrochemical determination and comparative analysis. J Appl Phys. 1984;55(8): 2977–2985. DOI: 10.1063/1.333358

[39] Zhou H, Qu Y, Zeid T, Duan X. Towards highly efficient photocatalysts using semiconductor nanoarchitectures. Energy Environ Sci. 2012;5(5):6732–6743. DOI: 10.1039/c2ee03447f

[40] Pradhan SK, Reucroft PJ, Yang F, Dozier A. Growth of TiO_2 nanorods by metalorganic chemical vapor deposition. J Crystal Growth. 2003;256(1):83–88. DOI: 10.1016/S0022-0248(03)01339-3

[41] Nian J-N, Teng H. Hydrothermal synthesis of single-crystalline anatase TiO2 nanorods with nanotubes as the precursor. J Phys Chem B. 2006;110(9):4193–4198. DOI: 10.1021/jp0567321

[42] González-García L, González-Valls I, Lira-Cantu M, Barranco A, González-Elipe AR. Aligned TiO2 nanocolumnar layers prepared by PVD-GLAD for transparent dye sensitized solar cells. Energy Environ Sci. 2011;4(9):3426–3435. DOI: 10.1039/c0ee00489h

[43] He Y, Zhang Z, Zhao Y. Optical and photocatalytic properties of oblique angle deposited TiO2 nanorod array. J Vacuum Sci Technol B: Microelectronics Nanometer Struct. 2008;26(4):1350–1358. DOI: 10.1116/1.2949111

[44] Wolcott A, Smith WA, Kuykendall TR, Zhao Y, Zhang JZ. Photoelectrochemical water splitting using dense and aligned TiO2 nanorod arrays. Small. 2009;5(1):104–111. DOI: 10.1002/smll.200800902

[45] Krause KM, Taschuk MT, Harris KD, Rider DA, Wakefield NG, Sit JC, et al. Surface area characterization of obliquely deposited metal oxide nanostructured thin films. Langmuir. 2009;26(6):4368–4376. DOI: 10.1021/la903444e

[46] Lee HJ, Chen P, Moon SJ, Sauvage F, Sivula K, Bessho T, et al. Regenerative PbS and CdS quantum dot sensitized solar cells with a cobalt complex as hole mediator. Langmuir. 2009;25(13):7602–7608. DOI: 10.1021/la900247r

[47] Zewdu T, Clifford JN, Hernandez JP, Palomares E. Photo-induced charge transfer dynamics in efficient TiO2/CdS/CdSe sensitized solar cells. Energy Environ Sci. 2011;4(11):4633–4638. DOI: 10.1021/la900247r

[48] Sun PP, Zhang XT, Wang CH, Wei YA, Wang LL, Liu YC. Rutile TiO2 nanowire array infiltrated with anatase nanoparticles as photoanode for dye-sensitized solar cells: enhanced cell performance via the rutile-anatase heterojunction. J Mater Chem A. 2013;1(10):3309–3314. DOI: 10.1021/la900247r

[49] Li ZC, Zhu Y, Zhou Q, Ni J, Zhang ZJ. Photocatalytic properties of TiO2 thin films obtained by glancing angle deposition. Appl Surf Sci. 2012;258(7):2766–2770. DOI: 10.1016/j.apsusc.2011.10.129

[50] Cheng P, Deng C, Gu M, Shangguan W. Visible-light responsive zinc ferrite doped titania photocatalyst for methyl orange degradation. J Mater Sci. 2007;42(22):9239–9244. DOI: 10.1007/s10853-007-1902-5

[51] Jin SF, Li YZ, Xie H, Chen X, Tian TT, Zhao XJ. Highly selective photocatalytic and sensing properties of 2D-ordered dome films of nano titania and nano Ag2+ doped titania. J Mater Chem. 2012;22(4):1469–1476. DOI: 10.1039/c1jm14216j

[52] Xie Y, Ali G, Yoo SH, Cho SO. Sonication-assisted synthesis of CdS quantum-dot-sensitized TiO2 nanotube arrays with enhanced photoelectrochemical and photocatalytic activity. Acs Appl Mater Inter.2(10):2910–2914. DOI: 10.1021/am100605a

[53] Tang WZ, Huang CP. Photocatalyzed oxidation pathways of 2,4-dichlorophenol by Cds in basic and acidic aqueous-solutions. Water Res. 1995;29(3):745–756. DOI: 10.1016/0043-1354(94)00151-V

[54] Yu K, Lin X, Lu GH, Wen ZH, Yuan C, Chen JH. Optimized CdS quantum dot-sensitized solar cell performance through atomic layer deposition of ultrathin TiO2 coating. Rsc Adv. 2012;2(20):7843–7848. DOI: 10.1039/c2ra20979a

[55] Roelofs KE, Brennan TP, Dominguez JC, Bailie CD, Margulis GY, Hoke ET, et al. Effect of Al2O3 recombination barrier layers deposited by atomic layer deposition in solid-state CdS quantum dot-sensitized solar cells. J Phys Chem C. 2013;117(11):5584–5592. DOI: 10.1021/jp311846r

[56] Kang Q, Cao JY, Zhang YJ, Liu LQ, Xu H, Ye JH. Reduced TiO2 nanotube arrays for photoelectrochemical water splitting. J Mater Chem A. 2013;1(18):5766–5774. DOI: 10.1039/c3ta10689f

[57] Kang Q, Cao J, Zhang Y, Liu L, Xu H, Ye J. Reduced TiO 2 nanotube arrays for photo-electrochemical water splitting. J Mater Chem A. 2013;1(18):5766–5774. DOI: 10.1039/c3ta10689f

[58] Hu Y, Song X, Jiang SM, Wei CH. Enhanced photocatalytic activity of Pt-doped TiO2 for NOx oxidation both under UV and visible light irradiation: A synergistic effect of lattice Pt4+ and surface PtO. Chem Eng J. 2015;274:102–112. DOI: 10.1016/j.cej.2015.03.135

[59] Ingram DB, Linic S. Water splitting on composite plasmonic-metal/semiconductor photoelectrodes: evidence for selective plasmon-induced formation of charge carriers near the semiconductor surface. J Am Chem Soc. 2011;133(14):5202–5205. DOI: 10.1021/ja200086g

[60] Meng ZD, Zhu L, Choi JG, Chen ML, Oh WC. Effect of Pt treated fullerene/TiO2 on the photocatalytic degradation of MO under visible light. J Mater Chem. 2011;21(12):7596–7603. DOI: 10.1039/c1jm10301f

[61] Pu YC, Wang GM, Chang KD, Ling YC, Lin YK, Fitzmorris BC, et al. Au Nanostructure-decorated TiO2 nanowires exhibiting photoactivity across entire UV-visible region for photoelectrochemical water splitting. Nano Lett. 2013;13(8):3817–3823. DOI: 10.1021/nl4018385

[62] Kominami H, Tanaka A, Hashimoto K. Mineralization of organic acids in aqueous suspensions of gold nanoparticles supported on cerium(IV) oxide powder under visible light irradiation. Chem Commun. 2010;46(8):1287–1289. DOI: 10.1039/b919598j

[63] Szabo Z, Furo I, Csoregh I. Combinatorial multinuclear NMR and X-ray diffraction studies of uranium(VI)-nucleotide complexes. J Am Chem Soc. 2005;127(43):15236–15247. DOI: 10.1021/ja0550273

[64] Trasatti S. Work function, electronegativity, and electrochemical behaviour of metals. 2. Potentials of zero charge and electrochemical work functions. J Electroanal Chem. 1971;33(2):351. DOI: 10.1016/0368-1874(71)80045-X

[65] Di Valentin C, Selloni A. Bulk and surface polarons in photoexcited anatase TiO2. J Phys Chem Lett. 2011;2(17):2223–2228 . DOI: 10.1021/jz2009874